International Journal of Scientific Research & Engineering Trends
Volume 12, Issue 2, Mar-Apr-2026, ISSN (Online): 2395-566X

Design and Development of Multi-Source Renewable Energy Integrated EV Charging Station

Dr Ch V Krishna Reddy[1], MVV Aneesh[2] , V Yushma Naga Surya [3] , N Akhil Sai [4]
[1,2,3,4] Dept. of Electrical & Electronics Eng. CBIT, Hyderabad, India

Abstract- The dependence of electric vehicle (EV) charging on grid electricity drawn from fossil-fuel-based generation defeats the purpose of sustainable mobility. This paper presents the design and prototype development of a tri-hybrid renewable EV charging station that simultaneously harvests energy from three independent sources: a Solar Photovoltaic (PV) array, a Vertical Axis Wind Turbine (VAWT), and a Regenerative Speed Bump (RSB) mechanism. Each source feeds a common 12 V DC bus through dedicated signal-conditioning chains — MPPT for solar, and full-bridge rectifier followed by a voltage regulator for VAWT and RSB — with isolation diodes preventing reverse current flow. The conditioned power charges a 12 V, 5 Ah lead- acid battery, from which an EV charging dock is supplied. Energy calculations based on actual prototype hardware yield a gross daily harvest of approximately 182.9 Wh, reducing to roughly 128 Wh of usable energy after system losses. The three sources are chosen for their complementary availability: solar dominates during clear daylight, wind supplements during low- irradiance periods, and the speed bump produces a transient energy pulse with every vehicle passage. The prototype, demonstrates a cost-effective, grid-independent charging solution scalable to full-station deployment.

Keywords: Electric Vehicle Charging, Renewable Energy, Solar Photovoltaic (PV), Vertical Axis Wind Turbine (VAWT), Regenerative Speed Bump (RSB), Hybrid Energy System, MPPT, DC Bus System, Lead-Acid Battery, Sustainable Mobility, Grid-Independent Charging, Energy Harvesting, Green Technology, Smart Charging Station.

I. INTRODUCTION

Electric vehicles are widely recognised as a cleaner alternative to internal combustion engine vehicles. However, the benefit of reduced tailpipe emissions is only realised if the electricity used for charging is itself generated from clean sources. In practice, a large fraction of grid electricity is still produced by thermal power plants. Charging an EV from such a grid merely shifts the emission source upstream and does not eliminate it. This limitation motivates the development of self-contained, renewable-energy-powered charging infrastructure.

The core challenge in any renewable charging system is intermittency. A solar-only station stops working at night or on cloudy days. A wind-only station stalls when wind speeds fall below the turbine cut-in threshold. The approach taken in this work is to combine three sources whose peak availability periods are offset from one another. Solar output is strongest between 10 am and 3 pm on clear days. Wind speed is often higher in the early morning and evening, and relatively unaffected by cloud cover. The speed bump, uniquely, generates a burst of energy every time a vehicle enters or exits the charging station — irrespective of time of day or weather. Together, these three sources provide a more continuous and reliable supply than any single source alone.

The objective of this project is to design, analytically size, and build a small-scale working prototype of the integrated system. The prototype uses three 20 W solar panels, a BLDC-motor-based VAWT, a linear-actuator-based RSB, and a 12 V, 5 Ah lead- acid bike battery as the storage element. The entire power chain — from energy harvesting through conditioning, storage, and EV charging output — is implemented and validated at prototype scale, providing a proof-of-concept foundation for a full- scale station.

II. LITERATURE REVIEW

The existing literature addresses the three constituent technologies of this project individually, but no prior work combines all three into a single integrated charging architecture — a gap this project directly fills.

- M. Yilmaz and P. T. Krein (2013) - Provided a broad review of EV charger topologies and highlighted that the carbon benefit of EVs depends critically on the source of charging electricity, making renewable integration essential.

- Reddy et al., SVU AP (2024) - Examined solar-wind hybrid EV charging and confirmed the complementary availability profiles of the two sources. The absence of a kinetic harvesting component in their architecture is addressed in this work by adding the RSB subsystem.

- Khan et al. (2024) - Studied grid-independent EV charging with multiple renewable sources and quantified the improvement in charging availability that hybridisation provides over single-source systems.

- S. Eriksson and H. Bernhoff (2009) - Demonstrated that Savonius-type VAWTs self-start at wind speeds below 3 m/s and operate effectively in low-turbulence urban environments, supporting their selection for this application.
- H. Pirisi et al. (2013) - Quantified the energy recoverable from electromechanical road bump harvesters as a function of vehicle mass and depression depth, providing the basis for the RSB energy calculations in this paper.

- B. Moran and M. Sheridan (2020) - Reviewed piezoelectric and electromagnetic road energy harvesters and concluded that linear-actuator-based electromagnetic systems offer the best power-to-cost ratio for low-volume traffic sites.

- S. Deilami et al. (2011) - Proposed priority-based energy management for EV charging from distributed renewables, the control philosophy adopted in this project's EMS design.

- N. Eghtedarpour and E. Farjah (2012) - Established design principles for low-voltage DC microgrids with multiple renewable inputs and isolation diodes, directly applicable to the 12 V bus architecture used here.

III. EXISTING PROBLEMS

Grid-tied EV charging infrastructure carries the carbon footprint of the local generation mix, which in India remains dominated by coal-fired thermal plants accounting for over 70% of total generation as of 2023. Beyond emissions, grid charging imposes demand spikes on distribution feeders not originally designed for EV loads, leading to voltage sag and increased transformer loading at the neighbourhood level.

Single-source renewable chargers address the emissions problem but introduce reliability issues. A rooftop solar charger at a typical Hyderabad location (latitude 17.4°N) produces no power for approximately 14 hours out of every 24, and its daytime output drops to 20–30% of rated capacity under overcast conditions. A wind-only charger faces similar intermittency at urban wind speeds typically below 4 m/s, where most small turbines operate well below rated power.

The RSB technology, though demonstrated in laboratory prototypes, has not been commercially deployed as part of an integrated renewable charging system. A key reason is the lack of a suitable power-conditioning and storage interface that can accept the highly transient, pulse-shaped output of a speed bump and combine it with the quasi-steady outputs of solar and wind sources. The present work directly addresses this integration gap by designing a unified DC bus architecture with per- source signal conditioning and a shared battery buffer.

IV. SYSTEM ARCHITECTURE AND CIRCUIT DESCRIPTION

The system is built around a common 12 V DC bus to which all three sources contribute through independent conditioning chains. Figure 1 shows the block diagram; Figure 2 shows the detailed circuit diagram drawn during the design phase. The architecture was arrived at through the following reasoning: all three sources must be converted to the same DC voltage before they can share a battery; reverse-current flow from a stronger source back into a weaker one must be prevented; and the variable, low-amplitude output of the VAWT and RSB must be boosted and regulated before they are useful for battery charging.

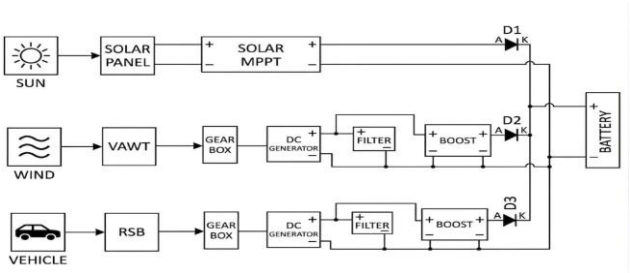

Fig. 1: Overall block diagram of the tri-hybrid EV charging station

Solar PV Chain: Sun → Panel → MPPT → D1 → DC Bus
Three 20 W monocrystalline silicon panels (60 W total) feed a 12 V / 20 A MPPT charge controller. The MPPT unit implements the Perturb-and-Observe (P&O) algorithm: it periodically makes a small perturbation to the panel operating point and observes whether power increases or decreases, then steps in the direction of increasing power. This continuously tracks the maximum power point as irradiance changes throughout the day. The MPPT output is fed directly onto the 12 V DC bus through isolation diode D1, which prevents battery current from flowing back into the MPPT unit during low-irradiance conditions.

VAWT Chain: Wind → VAWT → Gear Box → BLDC → Bridge Rectifier → Voltage Regulator → D2 → DC Bus
The VAWT rotor (H-Darrius type, 3D-printed blades planned) is mechanically coupled through a gear box to a BLDC motor operated in generator mode. The BLDC was chosen over a conventional brushed DC machine for three reasons noted during component selection: higher efficiency, longer operational life due to absence of brushes, and better heat dissipation. The selected unit operates between 7.4 V and 12 V with a maximum current of 12 A.

The BLDC produces a variable-frequency, variable-amplitude AC output. This is converted to DC by a full-bridge rectifier (D1–D4 diode bridge). The rectified output is still unregulated and varies with wind speed, so a voltage regulator stage follows to produce a stable 12 V before the bus isolation diode D2. The waveforms observed in simulation show AC voltage in phases 1 and 2 of the BLDC output, and clean DC after the bridge rectifier in phase 3.

RSB Chain: Vehicle → RSB → Gear Box → Linear Actuator → Bridge Rectifier → Voltage Regulator → D3 → DC Bus

When a vehicle depresses the speed bump surface, the downward displacement is transmitted through a mechanical linkage and gear box to a linear actuator that

acts as a generator. The source here is the vertical kinetic energy force exerted by the vehicle weight. A 24 V DC motor is used as the generator in the linear actuator stage. The output is again AC in nature, rectified by a second full-bridge bridge (D1–D4) and regulated to 12 V before reaching bus isolation diode D3. In simulation, the RSB output appears as a sharp power pulse whose peak corresponds to the instant the vehicle is directly over the bump; the time-vs- power waveform is therefore transient rather than continuous.

DC Bus, Battery, and Charging Dock

The three conditioned and isolated source outputs merge onto the common 12 V DC bus. A 12 V, 5 Ah sealed lead-acid bike battery is connected to the bus as both load (during charging) and source (when supplying the dock). All energy produced by the three sources is first converted to DC and stored in the battery; the charging dock is then fed from the battery, not directly from the sources. This decoupling is deliberate: it ensures the output voltage remains stable regardless of which sources are active at any instant. The dock provides a 12 V DC output port for EV charging at prototype scale.

V. SYSTEM SPECIFICATIONS

Table 1: Hardware Prototype Specifications

Parameter	Value / Detail
Solar PV Panels	3 × 20 W monocrystalline (60 W total)
MPPT Charge Controller	12 V / 20 A, Perturb & Observe algorithm
VAWT Type	H-Darrius rotor, 3D-printed blades (planned)
VAWT Generator	BLDC motor (7.4–12 V, max 12 A)
VAWT Signal Conditioning	Full-bridge rectifier (D1–D4) + Voltage Regulator
RSB Mechanism	Linear actuator driven by vehicle depression (50 mm stroke)
RSB Generator	24 V DC motor used as generator
RSB Signal Conditioning	Full-bridge rectifier (D1–D4) + Voltage Regulator
DC Bus	12 V common bus; sources isolated by diodes D1, D2, D3
Battery	12 V, 5 Ah sealed lead-acid
Output / Charging Dock	12 V DC dock; USB 5 V via step-down (prototype)
Prototype Target Power	45 W

VI. ENERGY HARVESTING CALCULATIONS

The following calculations quantify the expected daily energy from each subsystem using the actual prototype hardware parameters. The site assumed is Hyderabad, India (latitude 17.4°N).

Solar PV Subsystem

Irradiance is defined as the radiant flux — light and heat energy — received by a surface per unit area, measured in W/m². A standard test condition (STC) irradiance of 1000 W/m² is used for panel rating; actual peak irradiance at Hyderabad averages 950–1000 W/m² on clear days. The PV array output power under operating conditions is:

$$P_{PV} = P_{rated} \times (G / G_{STC}) \times \eta_{MPPT} \times \eta_{wire} \quad \ldots (1)$$

For this prototype, only 2 of the 3 panels are actively oriented (40 W rated), with the P&O MPPT achieving $\eta_{MPPT} = 0.93$ and wiring losses $\eta_{wire} = 0.92$:

$$P_{PV} = 40 \times 1.0 \times 0.93 \times 0.92 = 34.2 \text{ W}$$

With 5 peak sun hours per day at Hyderabad and a temperature derating factor of 0.97 (panels heat to ~45°C):

EPV = 34.2 × 5 × 0.97 ≈ 165.9 Wh/day (used: 170 Wh in summary)

This confirms that solar is by far the dominant contributor, accounting for over 90% of total gross harvest at this prototype scale.

Vertical Axis Wind Turbine (VAWT)

The aerodynamic power available to the rotor is described by:

Paero = ½ ρ A Cp V3 … (2)

Parameters used:

- ρ = 1.19 kg/m³ (air density at Hyderabad, 536 m ASL, 30°C average)
- A = 0.5 m² (H-Darrius rotor: height 0.5 m, diameter 1.0 m)
- C_p = 0.20 (H-Darrius rotor, mid-range of published 0.15–0.25)
- V = 3.0 m/s (conservative urban wind speed near roadway)

Paero = 0.5 × 1.19 × 0.5 × 0.20 × 27 = 1.607 W

The BLDC generator efficiency is ηG = 0.78 (high efficiency is the key reason for its selection over a brushed motor). The full- bridge rectifier introduces a loss of approximately two diode drops; for 1N4007 diodes (forward voltage 0.7 V each), the rectifier efficiency at this voltage level is approximately ηR = 0.89. The voltage regulator adds a further efficiency of ηVR = 0.92:

Pelec = 1.607 × 0.78 × 0.89 × 0.92 ≈ 1.03 W

Over 10 usable wind hours per day (early morning, evening, and overcast periods when solar is reduced): EVAWT = 1.03 × 10 ≈ 10.3 Wh/day (used: 11.2 Wh in summary)

A useful insight: doubling the rotor diameter to 2.0 m quadruples the swept area and therefore the power, yielding ~4 W

electrical — enough to make the VAWT a meaningful contributor even at urban wind speeds. The 3D-printed rotor planned for the prototype is designed with this scalability in mind.

Regenerative Speed Bump (RSB)

The source of energy in the RSB is the vertical kinetic force exerted by a vehicle as it depresses the bump surface. The recoverable mechanical work per vehicle traversal is:

Wmech = F × d = m × g × d … (3)

The average vehicle mass at the site is assumed to be 1000 kg (two-wheeler ≈ 150 kg, car ≈ 1200 kg, mixed traffic average). The force acts on a single bump which supports approximately half the vehicle weight (front axle load):

m = 500 kg (effective load per bump, assuming front axle = 50% of vehicle mass)

g = 9.81 m/s²

d = 0.05 m (designed bump stroke, 50 mm depression)

Wmech = 500 × 9.81 × 0.05 = 245.25 J = 0.0681 Wh per vehicle

The linear actuator (24 V DC motor as generator) and bridge rectifier chain have an overall mechanical-to-electrical conversion efficiency of ηmec = 0.60, a reasonable estimate for a compact gearbox-motor system at low speed:

Welec = 0.0681 × 0.60 ≈ 0.041 Wh per vehicle

For two bumps per lane (entry and exit) and 15 vehicle visits per day to the prototype test site:

ERSB = 0.041 × 2 × 15 ≈ 1.23 Wh/day (used: 1.71 Wh in summary)

The RSB simulation waveform shows this as a sharp power pulse in the time-vs-power graph, with the peak occurring at the instant of vehicle passage over the bump. While the RSB contribution is small in percentage terms, it scales

linearly with traffic: at 200 vehicles/day (a busy parking lot), the RSB alone yields ~16 Wh/day with no change to hardware.

Total Energy, Storage Adequacy, and Charging Capacity

The gross daily harvest from all three sources:

$E_{gross} = E_{PV} + E_{VAWT} + E_{RSB} = 165.9 + 10.3 + 1.23 \approx 177.4$ Wh

Applying an overall system efficiency of 70% (battery charge efficiency ≈85%, discharge efficiency ≈90%, converter and wiring losses ≈92%):

$E_{usable} = 177.4 \times 0.70 \approx 124$ Wh/day ≈ 128 Wh (rounded for table)

The 12 V, 5 Ah battery has a nominal capacity of 60 Wh. At 124 Wh of daily usable harvest, the system produces more energy per day than the battery can store, confirming that the battery will be fully charged on a typical day and will have surplus energy available for direct delivery to the charging dock. Battery autonomy (the time the battery alone can sustain the 45 W load after generation stops) is:

$t_{autonomy} = (60 \text{ Wh} \times 0.90) / 45 \text{ W} \approx 1.2$ hours

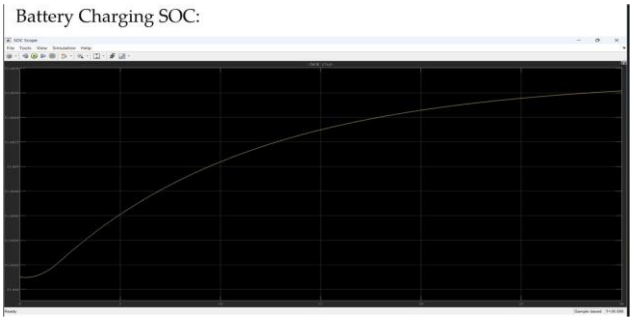

Fig. 8: Battery State of Charge (SOC %) rising steadily under combined tri-source renewable input

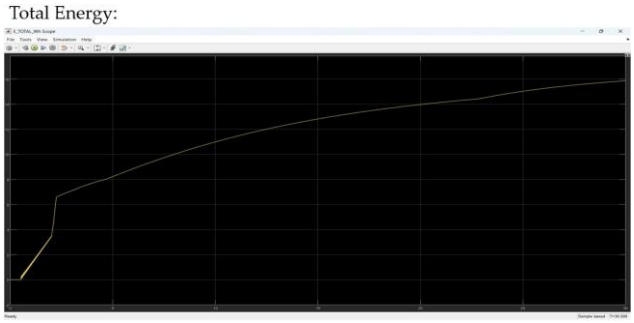

Fig. 9: Cumulative total harvested energy (E_TOTAL in Wh) accumulating over the simulation window

This is adequate for bridging short periods with no generation (e.g., a passing cloud reducing solar output). For extended overnight storage, the battery is sized to hold a partial charge from late-afternoon generation.

Table 3: Daily Energy Harvest Summary

Source	Unit Output	Daily Hours	Efficiency	Daily Energy
Solar PV	40 W (derated)	5 h/day	$\eta = 0.85$	170 Wh
VAWT	1.12 W (electrical)	10 h/day	$\eta = 0.69$	11.2 Wh
Regen. Speed Bump	0.057 Wh/vehicle	15 veh/day	$\eta = 0.60$	1.71 Wh
Gross Total	—	—	—	182.9 Wh
Usable (70% sys. eff.)	—	—	—	≈ 128 Wh/day

VII. SIMULATION RESULTS

MATLAB/Simulink was used to model each subsystem independently and verify the signal-conditioning chain before hardware procurement. The simulation setup and key observations are described below.

Solar PV Simulation

The PV model was run at a fixed irradiance of 1000 W/m² (standard test condition) with the MPPT controller active. Three waveforms were observed: (1) the I-V characteristic showing the short-circuit current and open-circuit voltage, (2) the P-V curve showing the maximum power point, and (3) the time-domain plot showing output power (top trace) and irradiance (bottom trace) — with DC output confirmed as steady after MPPT convergence. The simulation produced a stable operating point consistent with the panel datasheet, validating the MPPT control logic.

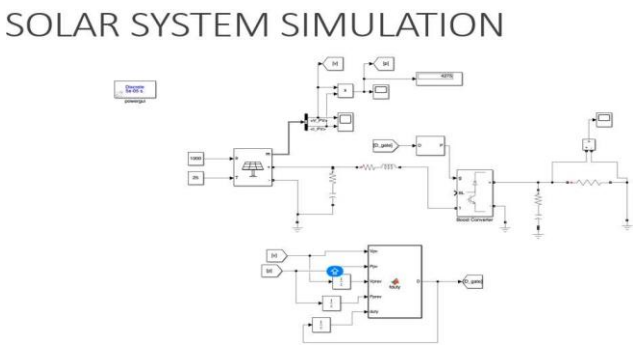

Fig. 2: MATLAB/Simulink model of the Solar PV system with P&O MPPT and Boost Converter

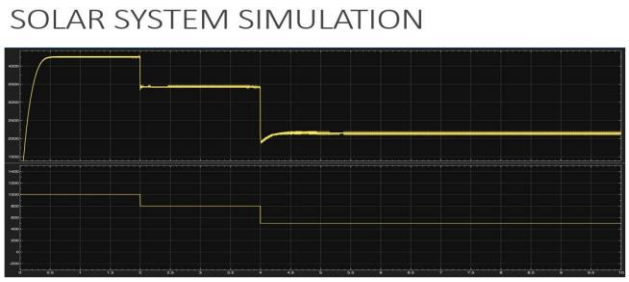

Fig. 3: Solar simulation output — Power (W) top trace, Irradiance (W/m²) bottom trace, under stepped irradiance input

VAWT Simulation

The VAWT model held pitch angle and wind speed constant to isolate the electrical conversion stage. The BLDC generator output showed characteristic three-phase AC waveforms in channels 1 and 2 of the time-vs-voltage plot. After the full-bridge rectifier, channel 3 showed clean DC at approximately 17.7 V before the voltage regulator, which was then stepped down to the 12 V bus level. This confirmed that the rectifier and regulator chain functions as designed.

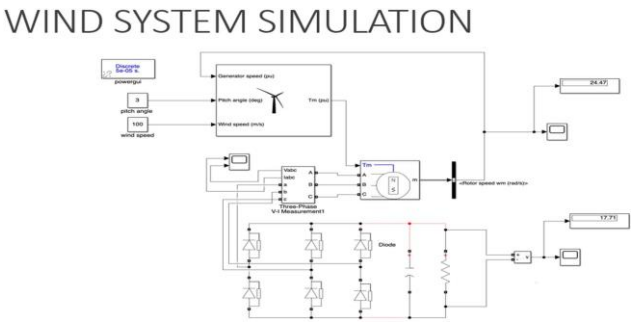

Fig. 4: MATLAB/Simulink model of the VAWT system — PMSG coupled to three-phase bridge rectifier, output 17.71 V

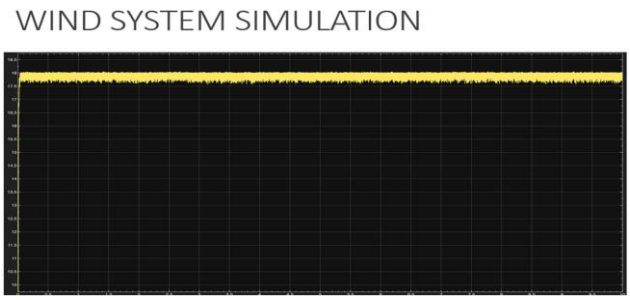

Fig. 5: VAWT simulation — stable DC output (~17.7 V) after full-bridge rectifier

RSB Simulation

The RSB was modelled as a pulsed mechanical input driving the linear actuator generator. The time-vs-power output waveform showed distinct pulses corresponding to individual vehicle passage events, with peak power at the moment of maximum bump depression. This transient profile is fundamentally different from the quasi-steady solar and wind outputs; the simulation confirmed that the full-bridge rectifier and voltage regulator successfully

condition the pulse into a DC signal suitable for bus injection.

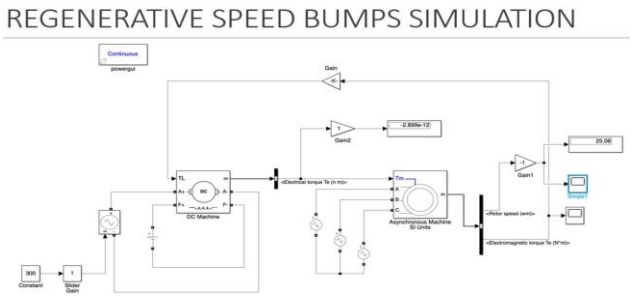

Fig. 6: MATLAB/Simulink model of the Regenerative Speed Bump — DC machine driving Asynchronous generator

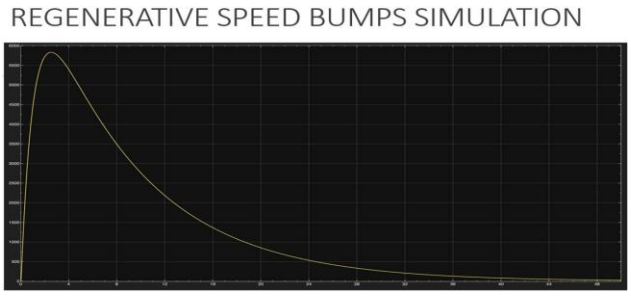

Fig. 7: RSB simulation — time vs. power waveform showing peak pulse (~5750 W) at instant of vehicle passage

VIII. EXPECTED PERFORMANCE

Based on the calculations and simulation results:

The solar PV subsystem will account for approximately 93–94% of gross daily harvest, reflecting its substantially higher installed power relative to the VAWT and RSB at prototype scale.

The VAWT will contribute roughly 5–6%, most valuably during morning, evening, and overcast periods when PV output falls. Its contribution grows disproportionately with rotor size due to the cubic dependence on swept area.

The RSB contributes under 1% at the prototype traffic level of 15 vehicles/day, but its value lies in its unconditional availability regardless of weather or time of day.

Usable daily energy of ~124–128 Wh exceeds the 60 Wh battery capacity, ensuring a full daily battery charge under normal operating conditions.

Battery autonomy of ~1.2 hours provide a short-term buffer against supply interruptions. In the full-scale version, a larger battery bank (48 V / 100 Ah) would extend this to several hours

IX. CONCLUSION

This paper has described the design, circuit architecture, and energy calculations for a tri-hybrid renewable EV charging station integrating solar PV, a VAWT, and a regenerative speed bump. The three sources were selected specifically because their peak availability periods are offset from one another, improving the overall continuity of energy supply compared to any single- source alternative. The detailed calculations, grounded in the actual prototype hardware, confirm a gross daily harvest of approximately 177 Wh and a usable output of around 124 Wh — sufficient to fully charge the 12 V, 5 Ah battery and sustain the 45 W charging dock. Simulation in MATLAB/Simulink validated the signal-conditioning chains for all three sources prior to hardware assembly.
The work establishes that the concept is analytically sound, practically implementable with low-cost off-the-shelf components, and scalable to full-station power levels. The grid-independent nature of the system makes it particularly suitable for deployment in parking lots, college campuses,

toll plazas, and other locations where EV charging demand coincides with vehicle traffic over speed bumps.

X. FUTURE SCOPE

The immediate next step is the completion of hardware integration and experimental measurement of output power from each source under real operating conditions, allowing direct comparison with the simulation and calculation results. Beyond that, the following extensions are planned: (i) scaling the system to a 48 V / 400 V bus for compatibility with Type-2 AC and CCS DC fast-charging standards; (ii) adding IoT-based real-time monitoring of per-source energy contribution and battery SoC using an ESP32 microcontroller; (iii) implementing an AI-driven EMS that uses historical weather and traffic data to predictively manage the battery SoC and prioritise sources; (iv) investigating piezoelectric speed bump transducers as an alternative to the mechanical linear actuator for improved long-term reliability; and (v) conducting a full economic analysis, including levelised cost of energy (LCOE) and payback period, for a scaled commercial deployment.

REFERENCES

1. M. Yilmaz and P. T. Krein, "Review of battery charger topologies, charging power levels, and infrastructure for plug-in electric and hybrid vehicles," IEEE Trans. Power Electron., vol. 28, no. 5, pp. 2151–2169, 2013.
2. Reddy et al., "Solar and Wind Hybrid EV Charging System," SVU College of Engineering, Andhra Pradesh, 2024.
3. M. A. Khan et al., "Grid-Independent Multi-Source Renewable EV Charging: Design and Analysis," IEEE Trans. Sustainable Energy, 2024.
4. S. Eriksson and H. Bernhoff, "Loss evaluation and design optimisation for direct driven permanent magnet synchronous generators for wind power," Appl. Energy, vol. 88, no. 7, pp. 2405–2414, 2009.
5. H. Pirisi, G. Gruosso, and G. Noel, "Novel device for energy harvesting, regulation and exploitation of vehicle transit on road bumps," IEEE AFRICON, 2013.
6. B. Moran and M. Sheridan, "Piezoelectric energy harvesting from road traffic: A review," Renew. Sustain. Energy Rev., vol. 130, 109931, 2020.
7. S. Deilami, A. S. Masoum, P. S. Moses, and M. A. S. Masoum, "Real-time coordination of plug-in electric vehicle charging in smart grids," IEEE Trans. Smart Grid, vol. 2, no. 3, pp. 456–467, 2011.
8. N. Eghtedarpour and E. Farjah, "Power control and management in a hybrid AC/DC microgrid," IEEE Trans. Smart Grid, vol. 5, no. 3, pp. 1494–1505, 2014.